Nano Energy 33 (2017) 29–36

Contents lists available at ScienceDirect

Nano Energy

journal homepage: www.elsevier.com/locate/nanoen

Full paper

A direct charger transfer from interface to surface for the highly efficient spatial separation of electrons and holes: The construction of Ti–C bonded interfaces in TiO_2-C composite as a touchstone for photocatalytic water splitting

Yurong Yang[a,b], Peng Gao[a,*], Ying Wang[a], Linna Sha[a], Xiaochen Ren[a], Jianjiao Zhang[a], Yujin Chen[c], Tingting Wu[a], Piaoping Yang[a], Xiaobo Li[a]

[a] *Key Laboratory of Superlight Materials and Surface Technology, Ministry of Education, College of Materials Science and Chemical Engineering, Harbin Engineering University, Harbin, Heilongjiang 150001, PR China*
[b] *College of Science, Heihe University, Heihe, Heilongjiang 164300, PR China*
[c] *College of Science, Harbin Engineering University, Harbin, Heilongjiang 150001, PR China*

ARTICLE INFO

Keywords:
Chemical connection
Ti–C bonds
Depletion layer
Charge separation
Photocatalytic water splitting for H_2

ABSTRACT

The construction of semiconductor composites is known a powerful method to realize the spatial separation of electrons and holes, which results in more electrons or holes dispersing on the surface, accompanying a charge transfer and further extending the region of charge depletion at the interface between these two components of the composite. However, most of them are based on a random accumulation connection of two different crystals and there are obvious empty spaces, which are formed as deplete layer to hinders the charge transfer to a large extent. In order to shorten the charger transfer path and make a direct charge transform from interface to surface, a chemically bonded interface in the composite is more reasonable. In this work, using one-dimensional TiO_2-C composite nanorods with a Ti–C chemically bonded interface as a touchstone, which was prepared through a simple carbonized process, the above strategy for better semiconductor photocatalytic water splitting property has been realized.

1. Introduction

In recent years, semiconductor photocatalysis have emerged as an important material in converting solar irradiation to hydrogen energy [1–3]. However, there two most important problems to be resolved: **I**) Engineering the semiconductor's band-gap for the visible-light absorption. In order to deal with this, many efficient works based on the compositing or doping method have been conducted [4–6]; **II**) Providing more free electrons on the surface. Higher concentration of electrons favors the following redox reaction from the points of both kinetics and thermodynamics. The construction of suitable semiconductor composites is known a powerful method to realize the separation of electrons and holes, which results in more electrons or holes dispersing on the special surface, accompanying a charge transfer and further extending the region of charge depletion at the interface between these two components of the composite [7,8]. Up to now, many semiconductor composites composed of different elements, morphologies, or dispersion states have been reported with improved photocatalytic activities [3,9–11]. However, most of them are based on a random accumulation of two different materials and there are obvious empty spaces, which are formed as depletion layer to hinder the charge transfer to a large extent, additional energy is needed for the charge to cross the depletion layer [12,13], as shown in Scheme 1. A bonded structure based on a chemical connection is undoubtedly a feasible way to resolve the above problem, because the sufficient chemical connection will absolutely eliminate the depletion layer between the two different components in the composite, as shown in Scheme 1. In this work, using one-dimensional TiO_2-C composite nanorods with a Ti–C chemically bonded interface as a touchstone, the above strategy for better semiconductor photocatalytic water splitting property has been validated.

Among a large variety of semiconductor materials, titanium dioxide (TiO_2) has been proven to be one of the most excellent photocatalyst for water splitting due to its good chemical stability, low cost, non-toxicity, and abundance in nature [4–6]. However, the photocatalytic efficiency of pristine TiO_2 is quite low because of its large band gap and high

* Corresponding author.
E-mail addresses: gaopeng@hrbeu.edu.cn (P. Gao), yangpiaoping@hrbeu.edu.cn (Y. Chen), chenyujin@hrbeu.edu.cn (P. Yang).

http://dx.doi.org/10.1016/j.nanoen.2017.01.030
Received 10 November 2016; Received in revised form 23 December 2016; Accepted 11 January 2017
Available online 13 January 2017

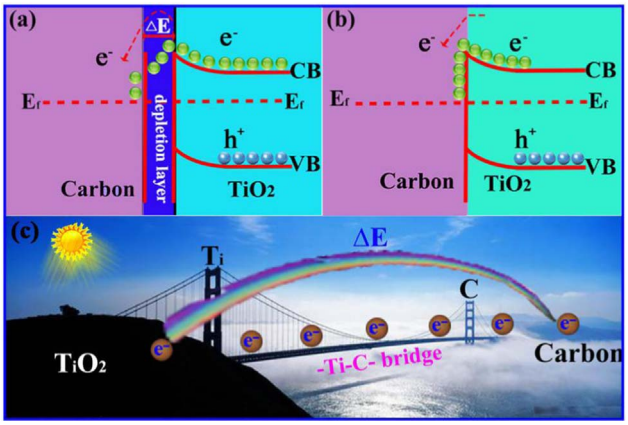

Scheme 1. The charge transfers in TiO_2-C and TiO_2/C nanorods. (a) TiO_2/C nanorods without a chemically bonded interface; (b) TiO_2-C nanorods with a chemically bonded interface; (c) The role of Ti–C bond in the separation of electron and hole.

recombination rate: approximately 90% of the photoelectrons and holes generated in it recombine within 10 ns [14]. In the past decades, significant efforts have been devoted to resolving the above problems, such as scale-downing the particle size to nanometer, doping with metal or non-metal, constructing heterostructure [15–18]. Among those, carbon modified TiO_2 composite materials exhibit outstanding solar-driven hydrogen production activities because of their relatively rapid separation and transfer of photo-induced carriers depended on the carbon materials' excellent conductivities [19–23]. However, though some works have proved the formation of Ti–C chemical bonds between TiO_2 and carbon materials [24–28], the utilization of this chemically bonded interface for promoting its photocatalytic water splitting property is not reported. Based on the theory analysis in Scheme 1, this special composite structure will efficiently facilitate the interfacial electron transfer and electron-hole separation due to suppressing the potential barrier (ΔE). In addition, the chemically bonded composite is more stable due to the strong chemical connection. Inspired by the important role of chemically bonded interface, we chose anatase TiO_2 nanorods as model semiconductor and used hydroquinone as the carbon source, and have constructed TiO_2-C core-shell nanorods with a Ti–C chemically bonded interface and TiO_2/C nanorods without a chemically bonded interface. And it was found that TiO_2-C nanorods achieved a 48.9% electron-hole separation efficiency under a 420 nm light and the carrier densities was up to 13.9×10^{18} cm^{-3}. As a result, the TiO_2-C nanorods' rate of visible-light driven photocatalytic water splitting for H_2 generation (7294 μmol h^{-1} g^{-1}) is about 12 times of that of TiO_2/C nanorods (605 μmol h^{-1} g^{-1}).

2. Results and discussions

2.1. Structures and compositions of the products

To study the chemical composition and valence state of the elements in the TiO_2, TiO_2-C and TiO_2/C samples, XPS analysis was conducted firstly. The full range of XPS spectra of TiO_2/C and TiO_2-C (Fig. S1), and Table S1 reveal that the sample is solely constituted of Ti, O and C in the absence of any contaminants. Fig. 1a, b and c show the Ti 2p and C 1s spectra of the raw TiO_2 and TiO_2-C nanorods, respectively. From Fig. 1b of the TiO_2-C sample, it can be seen that except two peaks centered at 458.6 and 464.5 eV of Ti $2p_{3/2}$ and Ti $2p_{1/2}$ [29], there are two additional peaks located at 460.3 eV and 466.2 eV compared with that of raw TiO_2, which are ascribed to the formation of a chemical bond (Ti–C bond) between titanium and carbon [30]. Accordingly, the formation of the Ti–C bonds is also confirmed by its C 1s spectra. As shown in Fig. 1c, the binding energy of 284.8 eV can be assigned to sp^2 hybridized carbon in the graphene state [28], and another two peaks centered at the binding energies of 286.5 and 288.6 eV are attributed to C–O and C=O bonds [31,32]. Moreover, a distinct peak located at 281.6 eV is also found, which further indicates the formation Ti–C bonds [33]. In addition, we do not found any peak corresponding to Ti^{3+}, which indicates that TiO_2 is not reduced in the hydroquinone carbonization process. Compared with the XPS results of TiO_2-C, the formation of Ti–C bond is not found in that of TiO_2/C sample (Fig. S2). In addition to the above XPS analysis, energy dispersive X-ray spectroscopy (EDX) mapping is also carried out to verify the element distribution in the as-expected TiO_2-C sample. As shown in Fig. 1d-g, it clearly shows that Ti, O and C elements are distributed uniformly in a typical TiO_2-C nanorod, which confirms the full coverage of carbon on the sample.

The compositions of the resultant samples are further characterized by XRD measurements, as shown in Fig. 2a. In Fig. 2a, it can be clearly seen that all the diffraction peaks of the TiO_2, TiO_2-C and TiO_2/C samples are well indexed to an anatase phased TiO_2 (JCPDS No. 21-1272). From the corresponding enlarged profiles in Fig. 2b and S3, it can be observed that all diffraction peaks of the TiO_2-C nanorods slightly shift to higher degree compared with that of pristine TiO_2 and TiO_2/C, which should be ascribed to the shrink during the carbonization process and the stress induced by Ti–C bonds between TiO_2 and carbon layers. Raman spectroscopy examination is also used to confirm the carbon's status, as illustrated in Fig. 2c. The characteristics peaks located at 143 cm^{-1} (E_g), 392 cm^{-1} (B_{1g}), 512 cm^{-1} (A_{1g}+B_{1g}) and 633 cm^{-1} (E_g) are corresponded to anatase TiO_2 [34]. In the spectrum of TiO_2/C sample, two peaks centered at 1345 and 1558 cm^{-1} (Fig. 2c inset) are displayed and assigned to the D and G peaks of carbon, which confirms that amorphous carbon layer is successfully assembled on [35]. Compared with the carbon spectrum of TiO_2/C sample, it is obvious that the D and G peaks of the TiO_2-C sample shift rightly to 1379 and 1569 cm^{-1}, which is due to the stress induced by Ti–C bonds between TiO_2 and carbon layers [30]. In addition, from the integrated intensities ratios of D and G peaks (I_D/I_G), the ratio of the TiO_2-C sample is 1.04, which is bigger than that of TiO_2/C sample (0.99). The higher ratio indicates a weakly ordered graphitic microstructure induced by the stress originated from Ti–C bonds between TiO_2 and carbon layers. Fourier transform infrare (FTIR) spectra of the as-obtained TiO_2, TiO_2/C and TiO_2-C samples are shown in Fig. 2d. It is seen that a peak centered at 3402 cm^{-1} is ascribed to O-H stretching vibration originated in the surface -OH groups [36]; two peaks at 2927 and 1325 cm^{-1} are attributed to the C–H stretching vibration [37]; C–C stretching vibration at 1635 cm^{-1} of surficial carbon layer is also found [36]. Notably, compared with TiO_2/C, a different peak at 802 cm^{-1} of Raman spectrum of TiO_2-C sample is observed, indicating the formation of Ti–C bond [26]. In summary, all the above results prove the formation of Ti–C bond in the TiO_2-C sample.

To investigate the morphologies and microstructures of the samples, scanning electron microscopy (SEM), transmission electron microscopy (TEM) and high-resolution transmission electron microscopy (HRTEM) examinations are carried out. Fig. 3a and b show the typical SEM images of the TiO_2 and TiO_2-C nanorods respectively, in which it can be seen that the nanorods are ~20 nm in width and ~500 nm in length with a relative smooth surface. The inset in Fig. 3a and b are the TEM images of typical nanorods of TiO_2 and TiO_2-C samples, respectively. After carbonization, the diameter of TiO_2 nanorods increased from 16.7 to 17.4 nm (TiO_2-C sample) and 17.7 nm (TiO_2/C sample, Fig. S4), which demonstrates the carbon layers on surface of TiO_2 nanorods are fairly thin. Compared with TiO_2 nanorods, TiO_2-C nanorods become more rough, which will increase the effective surface area available for the photocatalytic reaction. It is also demonstrated by their N_2 adsorption–desorption isotherms, as shown in Fig. S5. The as-synthesized TiO_2-C sample shows a larger specific surface area (109.48 m^2 g^{-1}) compared with TiO_2 (83.76 m^2 g^{-1}) and TiO_2/C (96.16 m^2 g^{-1}) samples. This can be

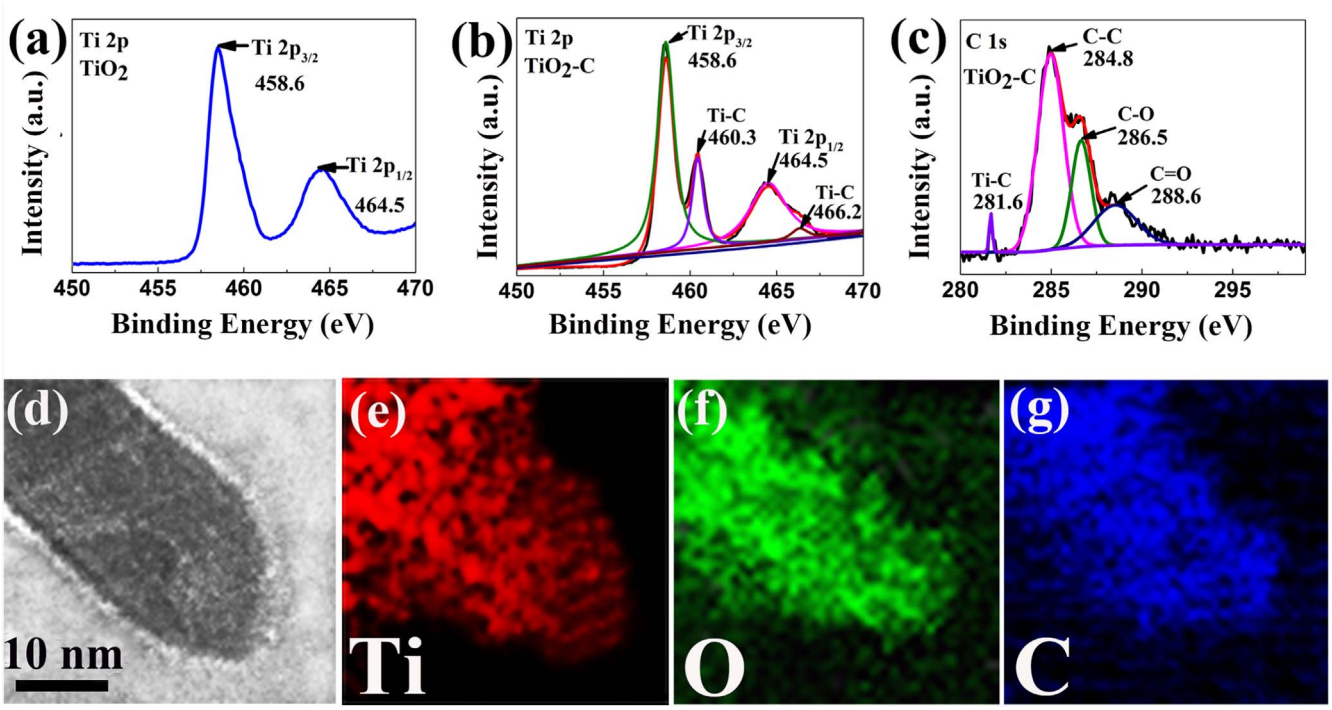

Fig. 1. XPS and TEM related examinations of TiO_2 nanorod precursor and TiO_2-C product. (a) Ti 2p spectra of the TiO_2 nanorod precursor; (b) and (c)Ti 2p and C 1 s spectra of the TiO_2-C nanorod sample; (d)-(g) TEM image of a typical TiO_2-C nanorod and its corresponding EDX element mappings of Ti, O and C elements.

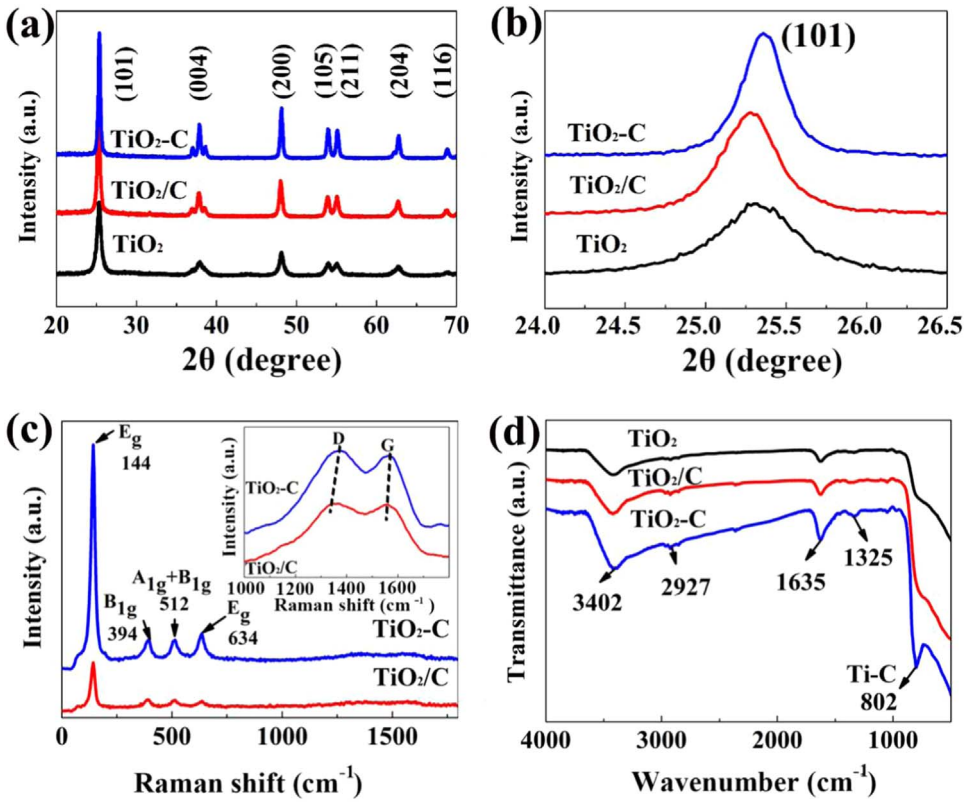

Fig. 2. (a) XRD patterns of TiO_2, TiO_2/C and TiO_2-C. (b) Enlarged (101) diffraction peaks in the above XRD patterns. (c) Raman spectra of TiO_2/C and TiO_2-C. (d) FTIR spectra of TiO_2, TiO_2/C and TiO_2-C.

ascribed to the deformed carbon layer of TiO_2-C sample pulled by the Ti-C bonds, which results in a more rough surface. It is also confirmed in Raman's results. The HRTEM images of TiO_2-C in Fig. 3c clearly reveals a lattice fringe spacing of 2.36 Å, corresponding to the (004) plane of anatase TiO_2. In contrast, regard to TiO_2/C, the lattice fringe spacing of (004) plane is 2.45 Å (Fig. S4). The above difference further discloses the compressive strain emanated from Ti–C bonds, which is consistent with their XRD results. Moreover, it is also observed that the carbon shell on the TiO_2-C surface is compose of 2 carbon atom-layers with a 3.36 Å d-spacing of the (002) plane of graphitic carbon.

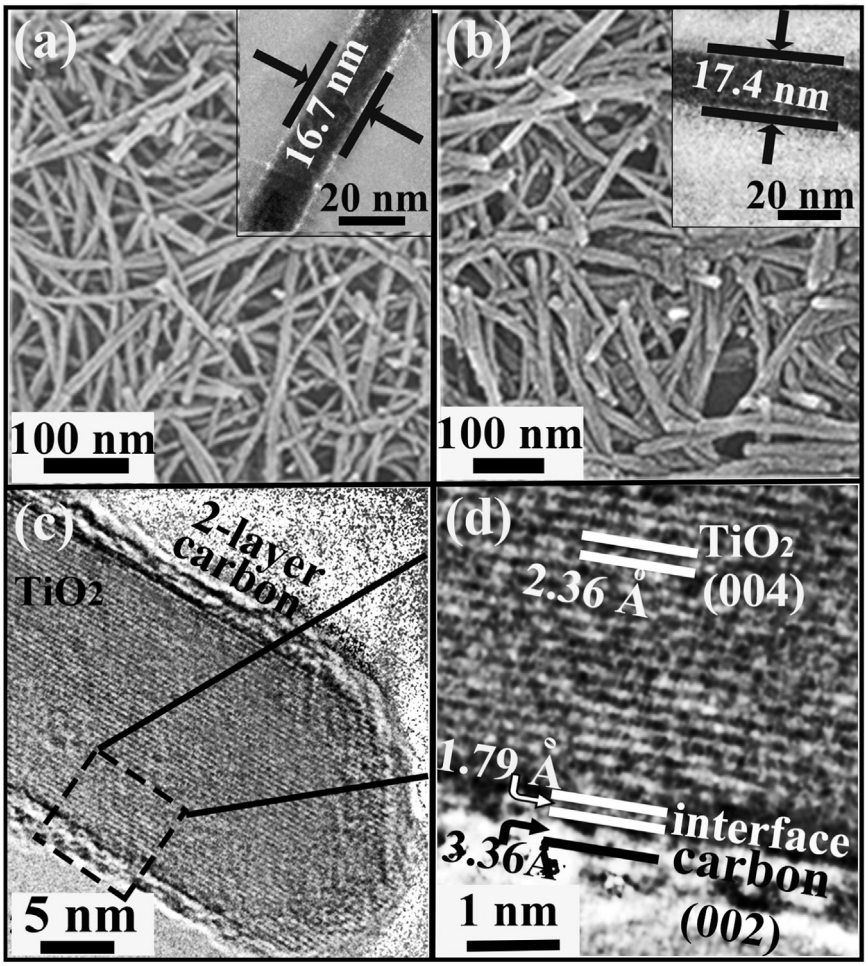

Fig. 3. (a) SEM image of TiO_2 nanorod precursor, the inset shows its TEM image of a typical nanorod; (b) SEM image of TiO_2-C nanorods, the inset shows its TEM image of a typical nanorod; (c) and (d) HRTEM image and its enlarged HRTEM image of a typical TiO_2-C nanorod.

Importantly, the distance from TiO_2 nanorod fringe to carbon sheet is 1.79 Å (Fig. 3d), which well agrees with the Ti–C chemical bond length reported in literature [38].

2.2. Chargers' separation in the products

To investigate the efficiency of charger separation and transportation in the as-obtained TiO_2 based semiconductors, photoluminescence (PL) measurements have been used firstly, as shown in Fig. 4a. It can be seen that the PL intensity at 320 nm of the unmodified TiO_2 is highest in three samples, which indicates the highest recombination rate of excited electron–holes. After modified by coating graphitic carbon, the recombination of an excited electron–hole in TiO_2 is effectively inhibited, remarkably so in TiO_2-C. This demonstrates that the chemically bonded interface in the TiO_2-C sample realize a highly efficient spatial separation of electrons and holes. Furthermore, we measured the charge separation efficiency through a method recently reported, in which H_2O_2 is used as a hole scavenger [39]. As shown in Fig. S6, it is found that the charge separation efficiency (CSE) of TiO_2/C sample is only 9.6% under visible-light irradiation (420 nm). In contrast, in the same conditions the CSE of TiO_2-C is elevated to 5 times (48.9%), which is much higher than that of TiO_2/C. After four cycles, the TiO_2-C sample still retains the initial high charge separation efficiency. Based on the above experimental results, it is affirmatively proved that Ti–C chemical bonds in TiO_2-C remarkably promote the separation of electrons and holes. After that, their photocurrent measurements are also performed at a fixed bias potential of 0.1 V. As depicted in Fig. 4b, the transient photocurrent density of the TiO_2 nanorods is only 0.08 mA cm^{-2}. After carbon coating, the photocurrent density of TiO_2 nanorods strongly improved (TiO_2/C: 0.17 mA cm^{-2}, TiO_2-C: 0.57 mA cm^{-2}). Notably, when light is switched on, the photocurrent respond of TiO_2-C is much faster than that of the TiO_2/C, implying that in TiO_2-C more electrons are generated and transferred due to the existence of Ti–C chemical bonds at their interface. As a complementary experiment, electrochemical impedance spectra (EIS) (Fig. 4c and d) are measured at a 5 kHz frequency in the dark and under a 420 nm irradiation. It is clear to seen that the arc radii under irradiation are much smaller than those in the dark. Under irradiation, TiO_2-C sample shows much smaller radii of the semicircular Nyquist plots compared to that of TiO_2/C, which further confirms the improved separation efficiency of electron hole-pairs in TiO_2-C nanorods [28,40]. To further ascertain the separation effect of electrons and holes in TiO_2/C and TiO_2-C nanorods, Zeta potential measurements via an on-off cycle of white-light irradiation are performed. As shown in Figs. S7 and S8, for TiO_2/C nanorods, its Zeta potential is centered at −2.64 eV when the light is off, which is relatively close to that of TiO_2-C nanorods (−2.85 eV). However, when the light is on, the Zeta potential of TiO_2-C nanorods is turned to −6.95 eV, which is much lower than that of TiO_2/C nanorods (−4.97 eV), confirming that more electrons are transferred onto the surface (carbon shell) in TiO_2-C nanorods. To further investigate the charge properties of the samples, a Mott-Schottky method has been used. Fig. S9 shows the Mott-Schottky plots of the samples obtained by us, characterizing that their Fermi level are about −0.88 and −0.61 V (vs NHE) for TiO_2/C and TiO_2-C, respectively. And the slopes of the plots are both positive, which indicate that they are n-type semiconductor. Additionally, from the slope of Mott-Schottky

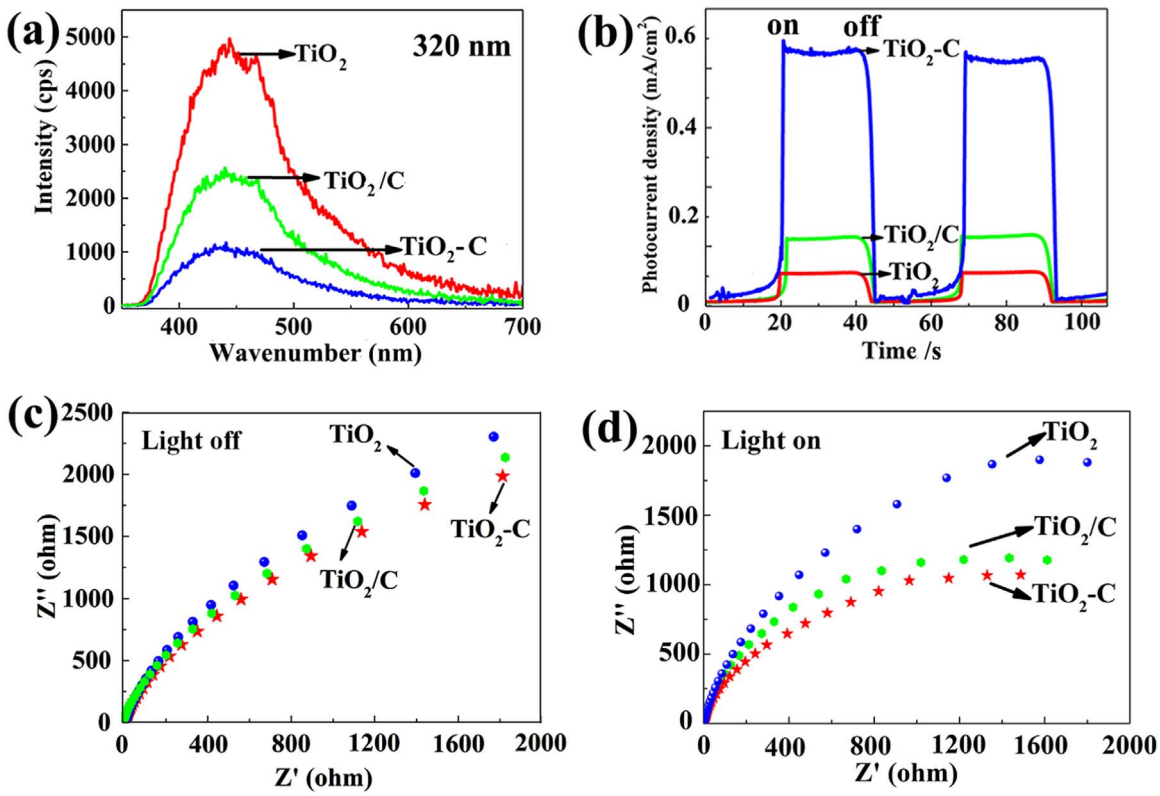

Fig. 4. (a) PL spectra of TiO_2, TiO_2/C and TiO_2-C; (b) Photocurrent density of TiO_2, TiO_2/C and TiO_2-C;(c) and (d) EIS Nyquist plots of the TiO_2, TiO_2/C and TiO_2-C in the dark and under irradiation.

plots, their carrier densities are calculated using the Equation [41]:

$$N_d = \frac{2}{e_0 \varepsilon \varepsilon_0} \Big/ \frac{d\,(1/C^2)}{dV} \tag{1}$$

where N_d and C are the carrier density and interfacial capacitance, respectively, e is the electronic charge, ε is the dielectric constant of the semiconductor, ε_O is the permittivity of free space, V is the applied voltage. The calculated carrier densities of TiO_2/C and TiO_2-C were 1.42×10^{18} and 13.9×10^{18} cm^{-3}, respectively. The higher the carrier density, the faster the carrier transport is. The carrier densities of TiO_2-C is about 10 times of that of TiO_2/C, so internal carrier transmission in TiO_2-C is faster, which also agrees with their photocurrent responses.

2.3. Photocatalytic properties of the products

To gain deeper insight into the electron transfer process, we have also characterized the energy band structures of TiO_2/C and TiO_2-C nanorods. Through a UV–vis DRS of TiO_2, TiO_2/C and TiO_2-C nanorods, as shown in Fig. 5a, it can be seen that the addition of carbon shell induces the increasement of visible light absorption, which is also found in previous studies [26–28]. More importantly, when Ti–C chemical bonds are introduced into the nanorods, the absorptions from UV region to visible-light region are obviously enhanced. Based on the plot of the transformed Kubelka-Munk function of UV–vis DRS (Fig. 5b and S10), the band gaps of TiO_2/C, TiO_2-C and TiO_2 are characterized as 3.18, 2.58 and 3.18 eV, respectively. The narrowed band gap with a decreased 0.6 eV in TiO_2-C is smaller than those previously reported in literatures of TiO_2 coated by carbon [21,22, 27], as shown in Table S2. It further confirms the advance of TiO_2-C composite. The energy band structures are further ascertained by XPS measurements. Their valence band (VB) spectra are shown in Fig. 5c. It is seen that the VB top of TiO_2/C and TiO_2-C are 1.10 and 0.77 eV below the Fermi level (E_F), respectively (Fig. 5c). After calibration with reference Fermi level, actual valence band values of TiO_2/C and TiO_2-C nanorods are 2.08 and 1.48 eV versus normal hydrogen electrode (NHE). Compared with TiO_2/C, TiO_2-C shows a 0.6 eV upward shift in the valence band top, which is the origin of the formation of Ti–C bonds. From the above determined VB tops and band gaps obtained in UV–vis absorption measurements, the energy band structures vs NHE of TiO_2/C nanorods and TiO_2-C nanorods are indexed, as shown in Fig. 5d. The narrowed VB should be due to the change of the electrons' status compared with pure TiO_2, which is induced by the hybridization of C 2p with Ti 3d orbitals. All the above experimental results and analysis indicate that the as-obtained TiO_2-C sample should have excellent photocatalytic property, especially for reducing reactions. So their catalytic abilities for hydrogen evolution through photocatalytic water-splitting process are measured. As shown in Fig. 5e, the H_2 evolution rate of TiO_2-C catalysis is around 7294 μmol h^{-1} g^{-1} and the quantum efficiency is 15.6% at 420 nm, which is significantly higher than those of TiO_2/C (605 μmol h^{-1} g^{-1}, 3.1%). Meanwhile, the TiO_2-C nanorods also retain high photocatalytic activity after ten cycles of 40 h reaction, which proves the catalytic stability of this material. Based on the above results, a mechanism for the photocatalytic water splitting for H_2 generation is proposed in Fig. 5f.

3. Conclusions

In summary, TiO_2-C nanorods with a Ti–C chemically bonded interface have been synthesized using TiO_2 nanorods as the template. As expected by us, an enhanced spatial separation of electrons and holes has been realized compared with TiO_2/C nanorods without Ti–C connnection, which results in more active electrons generated on the composite's surface for the following catalytic reaction. Therefore, the visible-light driven photocatalytic water splitting for H_2 generation based on TiO_2-C nanorods shows higher rate and good stability. This strategy for the spatial separation of electrons and holes based on the construction of chemical bond opens a new window for this field.

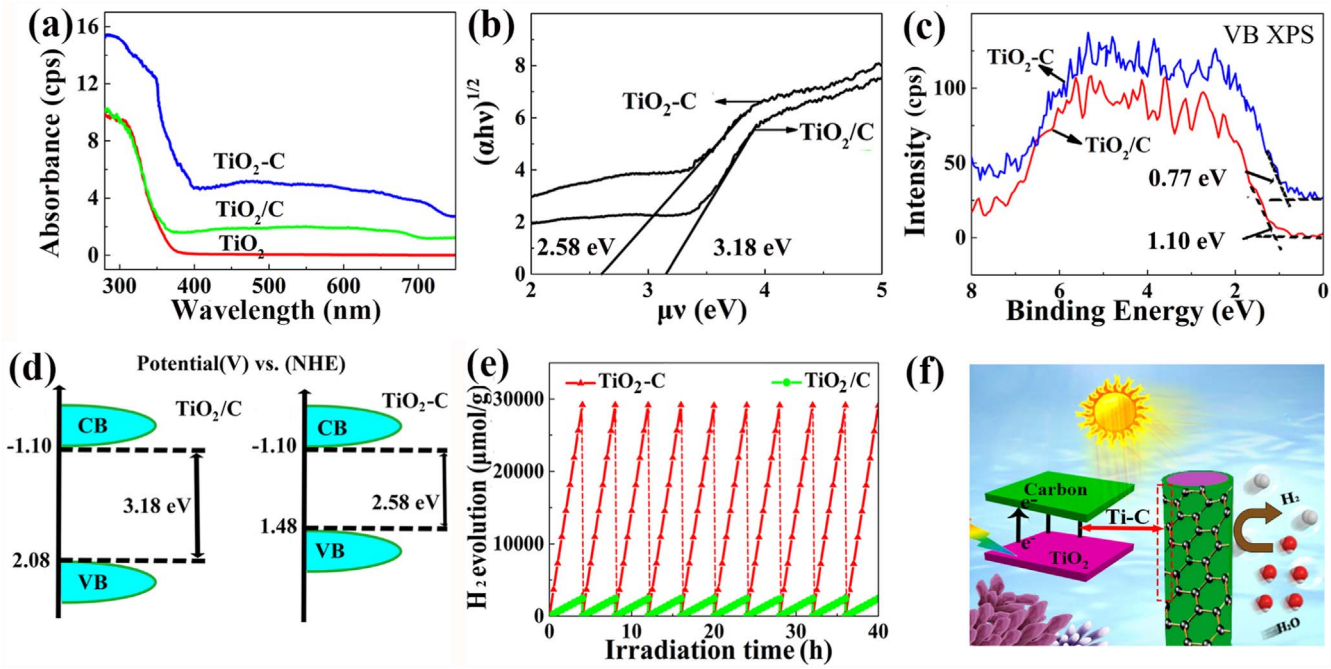

Fig. 5. (a) UV–vis DRS of TiO_2, TiO_2/C and TiO_2-C samples. (b) Optical band gaps determined by the UV–vis DRS. (c) Valence-band spectra measured by XPS. (d) The band structures of the TiO_2/C and TiO_2-C samples. (e) Visible-light driven photocatalytic water splitting for H_2 generation in 10 repeated cycles (4 h/cycle). (f) Proposed mechanism for the photocatalytic water splitting for H_2 generation of TiO_2-C sample.

4. Experimental section

4.1. Preparation of TiO_2 nanorods

All the chemicals were of analytical grade. TiO_2 nanorods were synthesized using an alkaline hydrothermal process. TiO_2 nanorods were synthesized according to the literature [42].

4.2. Preparation of TiO_2-C and TiO_2/C nanorods

TiO_2-C nanorods were prepared by a vacuum infiltration process. Based on previous study [43,44], it is easy to form -OH on the surface of TiO_2 nanorods by using water as the solvent in the heat treatment process, which is unfavourable for the formation of Ti–C chemical bonds between TiO_2 and carbon materials. Therefore, in this study, we use ethanol as solvent in the preparation of TiO_2-C nanorods. In a typical procedure, 0.4 g hydroquinone was mixed with 40 mL ethanol. After that, 1 g TiO_2 nanorods was added into the above solution under high purity nitrogen gas and stirred for 4 h. Then, a powder was collected by a filter process and washed with distilled water and ethanol for several times to remove excessive hydroquinone. Finally, the resulting sample was carbonized at 500 °C for 6 h under argon atmosphere with a heating rate of 5 °C min^{-1}. TiO_2/C nanorods were synthesized through a similar procedure, in which only water was used instead of ethanol.

Acknowledgements

We thank the Program for NCET in University (NCET-13-0754), Harbin Youth Fund (RC2013XK017003), Harbin Youth Fund (RC2014QN017004), the Fundamental Research funds for the Central Universities (2016), Youth Fund of Heilongjiang Province (QC2014C006) and Natural Science Foundation of Heilongjiang Province (B201603) for the financial support of this research.

Appendix A. Supplementary material

Supplementary data associated with this article can be found in the online version at doi:10.1016/j.nanoen.2017.01.030.

References

[1] X. Chen, S. Shen, L. Guo, S.M. Samuel, Chem. Rev. 110 (2010) 6503–6570.
[2] W.Y. Jiang, S. Bai, L.M. Wang, X.J. Wang, L. Yang, Y.R. Li, D. Liu, X.N. Wang, Z.Q. Li, J. Jiang, Y.J. Xiong, Small 12 (2016) 1640–1648.
[3] L. Li, J. Yan, T. Wang, Z.J. Zhao, J. Zhang, J. Gong, N. Guan, Nat. Commun. 6 (2015) 5881–5891.
[4] S. Hoang, S.P. Berglund, N.T. Hahn, A.J. Bard, C.B. Mullins, J. Am. Chem. Soc. 134 (2012) 3659–3662.
[5] Y.J. Yuan, Z.J. Ye, H.W. Lu, B. Hu, Y.H. Li, D.Q. Chen, J.S. Zhong, Z.T. Yu, Z.G. Zou, ACS Catal. 6 (2016) 532–541.
[6] D. Li, H. Haneda, N.K. Labhsetwar, S. Hishita, N. Ohashi, Chem. Phys. Lett. 401 (2005) 579–584.
[7] S.J.A. Moniz, S.A. Shevlin, D.J. Martin, Z.X. Guo, J. Tang, Energy Environ. Sci. 8 (2015) 731–759.
[8] X. Liu, G. Dong, S. Li, G. Lu, Y. Bi, J. Am. Chem. Soc. 138 (2016) 2917–2920.
[9] K. Woan, G. Pyrgiotakis, W. Sigmund, Adv. Mater. 21 (2009) 2233–2239.
[10] M.D. Hernández, F. Fresno, S. Suárez, J.M. Coronado, Energy Environ. Sci. 2 (2009) 1231–1257.
[11] X. Chen, S.M. Samuel, Chem. Rev. 107 (2007) 2891–2959.
[12] J. Zhou, Y. Gu, Y. Hu, W. Mai, P.H. Yeh, G. Bao, A.K. Sood, D.L. Polla, Z.L. Wang, Appl. Phys. Lett. 94 (2009) 191103.
[13] Y. Muraoka, N. Takubo, Z. Hiroi, J. Appl. Phys. 105 (2009) 103702–103707.
[14] J. Sun, Y. Yang, J.I. Khan, E. Alarousu, Z. Guo, X. Zhang, Q. Zhang, O.F. Mohammed, ACS Appl. Mater. Interfaces 6 (2014) 10022–10027.
[15] X. Wu, S. Yin, Q. Dong, C. Guo, T. Kimura, J. i. Matsushita, T. Sato, J. Phys. Chem. C 117 (2013) 8345–8352.
[16] Z. Fan, L. Wang, T. Wu, Z. Zhang, D. Borchardt, P. Feng, J. Am. Chem. Soc. 132 (2010) 11856.
[17] T. Sun, J. Fan, E. Liu, L. Liu, Y. Wang, H. Dai, Y. Yang, W. Hou, X. Hu, Z. Jiang, Powder Technol. 228 (2012) 210–218.
[18] H. Wang, L. Zhang, Z. Chen, J. Hu, S. Li, Z. Wang, J. Liu, X. Wang, Chem. Soc. Rev. 43 (2014) 5234–5244.
[19] S. Anandan, T.N. Rao, M. Sathish, D. Rangappa, I. Honma, M. Miyauchi, ACS Appl. Mater. Interfaces 5 (2013) 207–212.
[20] A. Du, Y.H. Ng, N.J. Bell, Z. Zhu, R. Amal, S.C. Smith, J. Phys. Chem. Lett. 2 (2011) 894–899.
[21] S. Sakthivel, H. Kisch, Angew. Chem. Int. Ed. 42 (2003) 4908–4911.
[22] Y. Zhang, Z.R. Tang, X. Fu, Y. Xu, ACS Nano 4 (2010) 7303–7314.
[23] J. Liu, H. Bai, Y. Wang, Z. Liu, X. Zhang, D.D. Sun, Adv. Funct. Mater. 20 (2010) 4175–4181.
[24] S.P. Debraj Ghosh, W. Chen, S. Chen, Chem. Mater. 20 (2008) 1248–1250.

[25] B.K. Vijayan, N.M. Dimitrijevic, D. Finkelstein, J. Wu, K.A. Gray, ACS Catal. 2 (2012) 223–229.
[26] X. Pan, Y. Zhao, S. Liu, C.L. Korzeniewski, S. Wang, Z. Fan, ACS Appl. Mater. Interfaces 4 (2012) 3944–3950.
[27] B. Li, Z. Zhao, F. Gao, X. Wang, J. Qiu, Appl. Catal. B 147 (2014) 958–964.
[28] Q. Huang, S. Tian, D. Zeng, X. Wang, W. Song, Y. Li, W. Xiao, C. Xie, ACS Catal. 3 (2013) 1477–1485.
[29] X. Shao, W. Lu, R. Zhang, F. Pan, Sci. Rep. 3 (2013) 3018.
[30] O. Akhavan, E. Ghaderi, J. Phys. Chem. C 113 (2009) 20214–20220.
[31] E.M. Rockafellow, X. Fang, B.G. Trewyn, K. Schmidt, W.S. Jenks, Chem. Mater. 21 (2009) 1187–1197.
[32] A. Choukourov, A. Grinevich, O. Polonskyi, J. Hanus, J. Kousal, D. Slavinska, H. Biederman, J. Phys. Chem. B 113 (2009) 2984–2989.
[33] P.Y. Jouan, M.C. Peignon, C. Cardinaud, G. Lempérière, Appl. Surf. Sci. 68 (1993) 595–603.
[34] S. Shanmugam, A. Gabashvili, D.S. Jacob, J.C. Yu, A. Gedanken, Chem. Mater. 18 (2006) 2275–2282.
[35] D. Zhang, F. Xie, P. Lin, W.C.H. Choy, ACS Nano 7 (2013) 1740–1747.
[36] R. Wang, Q. Wu, Y. Lu, H. Liu, Y. Xia, J. Liu, D. Yang, Z. Huo, X. Yao, ACS Appl. Mater. Interfaces 6 (2014) 2118–2124.
[37] E. Thiyagarajan, P. Saravanan, S. Shiyamala, P. Saranya, G.N. Nagendra, S. Renganathan, J. Saudi Chem. Soc. 5 (2013) 1–4.
[38] J. Huang, Q. Shang, Y. Huang, F. Tang, Q. Zhang, Q. Liu, S. Jiang, F. Hu, W. Liu, Y. Luo, T. Yao, Y. Jiang, Z. Pan, Z. Sun, S. Wei, Angew. Chem. Int. Ed. 55 (2016) 2137–2141.
[39] M. Adachi, M. Sakamoto, J. Jiu, Y. Ogata, S. Isoda, J. Phys. Chem. B 110 (2006) 13872–13880.
[40] K. Darowicki, S. Krakowiak, P. Ślepski, Electrochim. Acta 51 (2006) 2204–2208.
[41] Y. Xu, Y. Zhuang, X. Fu, J. Phys. Chem. C 114 (2010) 2669–2676.
[42] W. Liu, P. Gao, D. Bao, G. Zhang, Y. Chen, G. Chen, Y. Wang, L. Wang, S. Yang, G. Li, Y. Sun, RSC Adv. 3 (2013) 6531–6537.
[43] Y. Yu, J. Yu, J. Yu, Y. Kwok, Y. Che, J. Zhao, L. Ding, W. Ge, P. Wong, Appl. Catal. A 289 (2005) 186–196.
[44] F. Dong, S. Guo, H. Wang, X. Li, Z. Wu, J. Phys. Chem. . 115 (2011) 13285–13292.

Yurong Yang received her M.S. from Jilin Normal University in 2009. Currently she is pursuing her Ph.D. under the supervision of Prof. Peng Gao in College of Materials Science and Chemical Engineering at Harbin Engineering University. Her research is mainly focuses on nanomaterials for photo-catalysis and photoeletrocatalysis.

Peng Gao is currently a Professor of Chemistry in the College of Material Science and Chemical Engineering at Harbin Engineering University (Harbin, China). He received his B.S. and Ph.D. degree at University of Science and Technology of China. His research mainly focuses on the nanostructured materials for the energy storage and conversion systems.

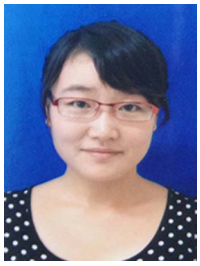

Ying Wang received her B.S. from Harbin Engineering University in 2011. Currently she is pursuing his Ph.D. under the supervision of Prof. Peng Gao in College of Materials Science and Chemical Engineering at Harbin Engineering University. Her research is mainly focuses on the metal-base compounds for hydrogen storage and nanostructured materials for hydrogen production.

Linna Sha received her undergraduate degree from Mudanjiang Normal University in 2015. Currently she is pursuing her Ph.D. under the supervision of Prof. Peng Gao in College of Materials Science and Chemical Engineering at Harbin Engineering University. Her research is mainly focuses on the nanomaterials for Lithium ion battery and photocatalytic hydrogen production.

Xiaochen Ren received her undergraduate degree from Shanxi Normal University in 2016. Currently is pursuing her M.S. under the supervision of Prof. Peng Gao at Harbin Engineering University. Her research is mainly focuses on photocatalysis hydrogen production by water splitting.

Jianjiao Zhang is a lecturer of Heilongjiang Institute of Technology. He received his Ph.D. degree in 2014 from Harbin University of Science and Technology. Currently he is pursuing his post-doctor research supervised by the professor Peng Gao in Harbin Engineering University. His current research mainly focuses on nanomaterials for hydrogen production and storage, electrochemical biosensor and gas sensor.

Yujin Chen has been a professor at Harbin Engineering University since 2007. He received his MS degree in 2003 from Harbin Engineering University and Ph.D. degree in 2005 from Chinese Academy of Science. His research interests focus on the nanostructured materials for the energy storage and conversion systems.

Tingting Wu received her B.S. degree from Hubei University in 2014. Currently she is a third-year graduate student of Prof. Peng Gao at Harbin Engineering University. Her research is mainly focuses on nanomaterials for photocatalysis and electromagnetic wave absorption.

Piaoping Yang is currently a Professor of Chemistry in the College of Material Science and Chemical Engineering at Harbin Engineering University (Harbin, China). He received his B.S. degree at Nankai University (Tianjin, China) and his Ph.D. degree at Jilin University (Changchun, China). After graduation, he joined Prof. Jun Lin's group for postdoctoral research. His research mainly focuses on the fabrication and biomedical applications of rare earth based functional materials.

Xiaobo Li received his B.S. degree from Heilongjiang University in 2014. Currently he is a third-year graduate student of Prof. Peng Gao at Harbin Engineering University. His research is mainly focuses on nanomaterials for photocatalysis and electrocatalytic hydrogen evolution.